ARTICLE • OPEN ACCESS

Numerical simulation on the effect of sample geometry size on the metal flow behaviour during the forging process

To cite this article: J Obiko and F Mwema 2020 *IOP SciNotes* **1** 014401

View the article online for updates and enhancements.

Recent citations

- Welcome to *IOP SciNotes*—a new open access journal for short research outputs across the physical and environmental sciences
Lauren Carter

IOP SciNotes

ARTICLE

Numerical simulation on the effect of sample geometry size on the metal flow behaviour during the forging process

J Obiko[1] ⬤ and F Mwema[2]

[1] Jomo Kenyatta University of Agriculture and Technology, Box 62000 Nairobi, Kenya
[2] Dedan Kimathi University of Technology, Private Bag, 10143 Nyeri, Kenya

E-mail: jobiko@jkuat.ac.ke

Abstract

This paper reports on the effect of sample geometry size on the metal flow behaviour using Deform^{TM} 3D finite element simulation software. The simulation process was done at forging temperature of 1100 °C and upper die speed of 50 mm/second. The friction coefficient between the die and the sample interface was taken to be constant during the simulation process. The results of the effective stress and strain distribution in the deformed sample were reported. The results show that the effective stress and strain distribution in the deformed sample was non-uniformly distributed. The maximum effective strain occurred at the centre of the deformed sample for all the samples tested. The maximum effective stress occurred at the die-sample contact surface. At the contact surfaces, the effective stress decreased with a decrease in the sample size. The effective stress at the centre of the deformed sample increased with a decrease in the sample geometry size.

1. Introduction

Structural components mostly used in the aerospace, automobile and power plant industries are fabricated by various thermo-mechanical processes such as forging, rolling and extrusion [1]. During deformation, metals and alloys are subjected to large plastic deformation [2]. In forging, the metal flow behaviour depends on the forging parameters such as, temperature, strain rate, the degree of deformation and the chemical composition of the material [3]. These parameters influence the microstructure evolution and the final product quality [1]. As such, an optimisation to thermo-mechanical processes will ensure that the produced components have the desired microstructure and free from deformation defects [1, 4].

Constitutive modelling has been widely used to study metal flow behaviour taking into account the effects of process parameters [4, 5]. The constitutive equations provide the intrinsic workability behaviour of the material during deformation [6]. The stress-strain state during deformation is complex [2], due to inhomogeneities effects of process parameters [4]. Physical simulations using the thermo-mechanical equipment have been applied to predict and simulate the metal forming processes [7–9]. Researchers have used different sample geometry size having the same aspect ratio of 1.5 to study the metal flow behaviour [3, 9, 10]. However, the validity of the obtained results has not been reported. In this study, Deform^{TM} 3D finite element simulation software has been used to study the metal flow behaviour during upsetting (forging) as affected by the sample geometry size. Four cylindrical samples of AISI 1045 steel were tested. The cylindrical samples had the same aspect ratio of 1.5 but with different geometry sizes.

The novelty of the article is based on the effect of geometry size on the flow stress analysis during forging, conspicuously missing in the literature. The information provides the basis for future arguments in approximating constitutive constants.

2. Simulation modelling

In this study, isothermal 3D forging simulation was done using Deform™ 3D finite element simulation software. In the simulation process, rigid-viscoplastic material has been considered as the workpiece material [11]. The

Figure 1. (a) Meshed and loaded finite element model, and (b) deformed specimen.
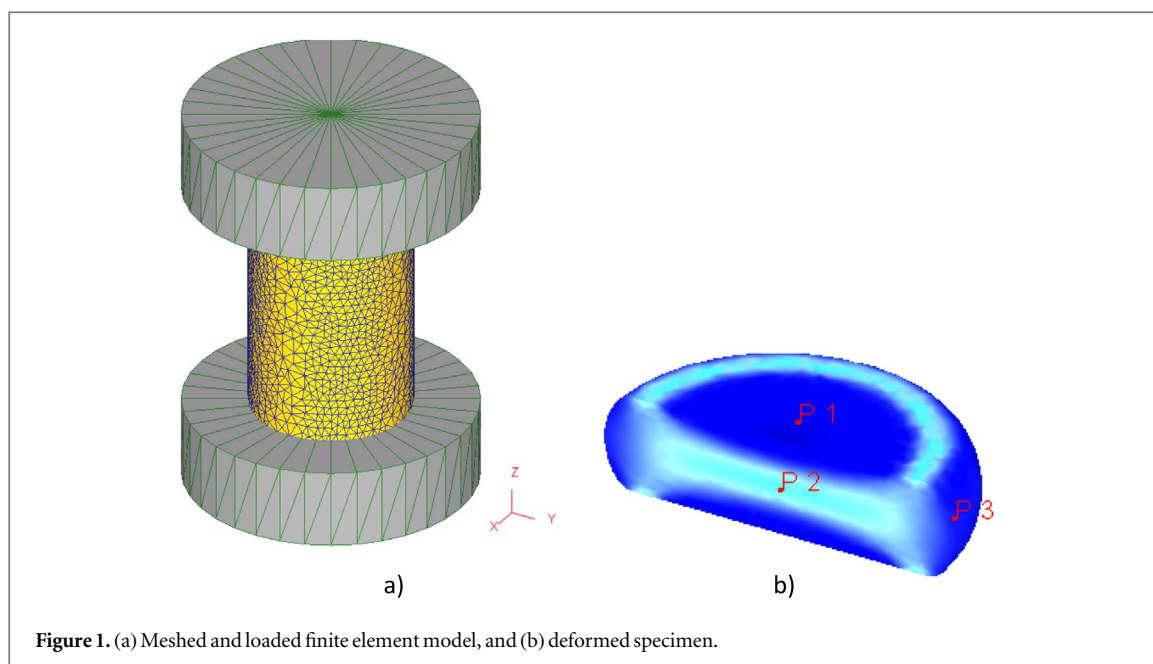
governing equations for forging simulation have been extensively covered in the literature. To avoid duplication, the readers are directed to our previous articles [12, 13] and other published articles [11, 14]. The simulation model of the cylindrical workpiece and the dies (upper and lower) were designed by in-built primitive geometry in the simulation software tool. The material for the workpiece (AISI 1045) and dies (carbide-15% cobalt) were selected from the software database. The FEM simulation model used is as shown in figure 1(a). The sample geometry sizes considered for forging had an initial height h_o (mm) to diameter d_o (mm) of 21 to 14 (sample 1), 18 to 12 (sample 2), 15 to 10 (sample 3) and 12 to 8 (sample4). The forging temperature of 1100 °C (workpiece) and the die temperature was set at 100 °C. In the simulation process, the workpiece was discretised into 34,527 tetrahedral mesh element and 7,088 nodes. The elements in the whole volume of the workpiece were refined to increase the accuracy of the results. In bulk deformation, the die-workpiece contact friction is taken to be of shear type. This is because of the deformed material experiences shear deformation during deformation. For forging, the friction values range between 0.2–0.9 [12]. The friction coefficient was taken to be 0.3 and of shear-type. The friction value (0.3) represent graphite lubrication for hot forging. The top die was set at a constant speed of 50 mm s^{-1}, and the final deformation was 67%.

3. Results and discussion

3.1. Effect of deformation degree on the effective strain

In this study, the coefficient of friction between the die and workpiece interface was assumed to be constant. From a practical view, the friction coefficient increases with the degree of deformation during compression test [13, 15]. The presence of interfacial friction results in inhomogeneous deformation hence leads to the formation of three zones in the deformed specimen as shown in figure 1(b) [16, 17]. The effective strain values were different in these regions.

Figure 2 shows the effective strain distribution in the deformed sample 4 at various deformation steps during forging simulation. The results show that the effective strain was inhomogeneous in the deformed sample. The maximum effective strain occurred at the centre of the specimen at point 2 as shown in figure 1(b). This region (point 2 as shown in figure 1(b)) experienced intense shear leading to grain refinement due to severe plastic deformation [16]. Research has shown that severe plastic deformation results in dynamic recrystallisation, hence finer grain structures are expected to form at point 2 [17]. The lowest effective strain occurred at the die-specimen contact surface (point 1). This was attributed to the resistance of frictional shear force to the lateral metal flow and the chilling effect of the blank [16, 18]. The drum-shaped region (point 3) experienced higher effective strain than point 1, but lower than point 2. The effective strain in this region (point 3) increased from the outer edge surface to the centre of the deformed specimen.

A similar trend in the effective strain across the deformed specimen was observed in the other three samples (sample 1, 2 and 3), but the contour maps are shown herein. This was to avoid duplication of contour maps even though the effective strain values were different.

Figure 2. An effective strain distribution at varoius deformation steps for sample 4.
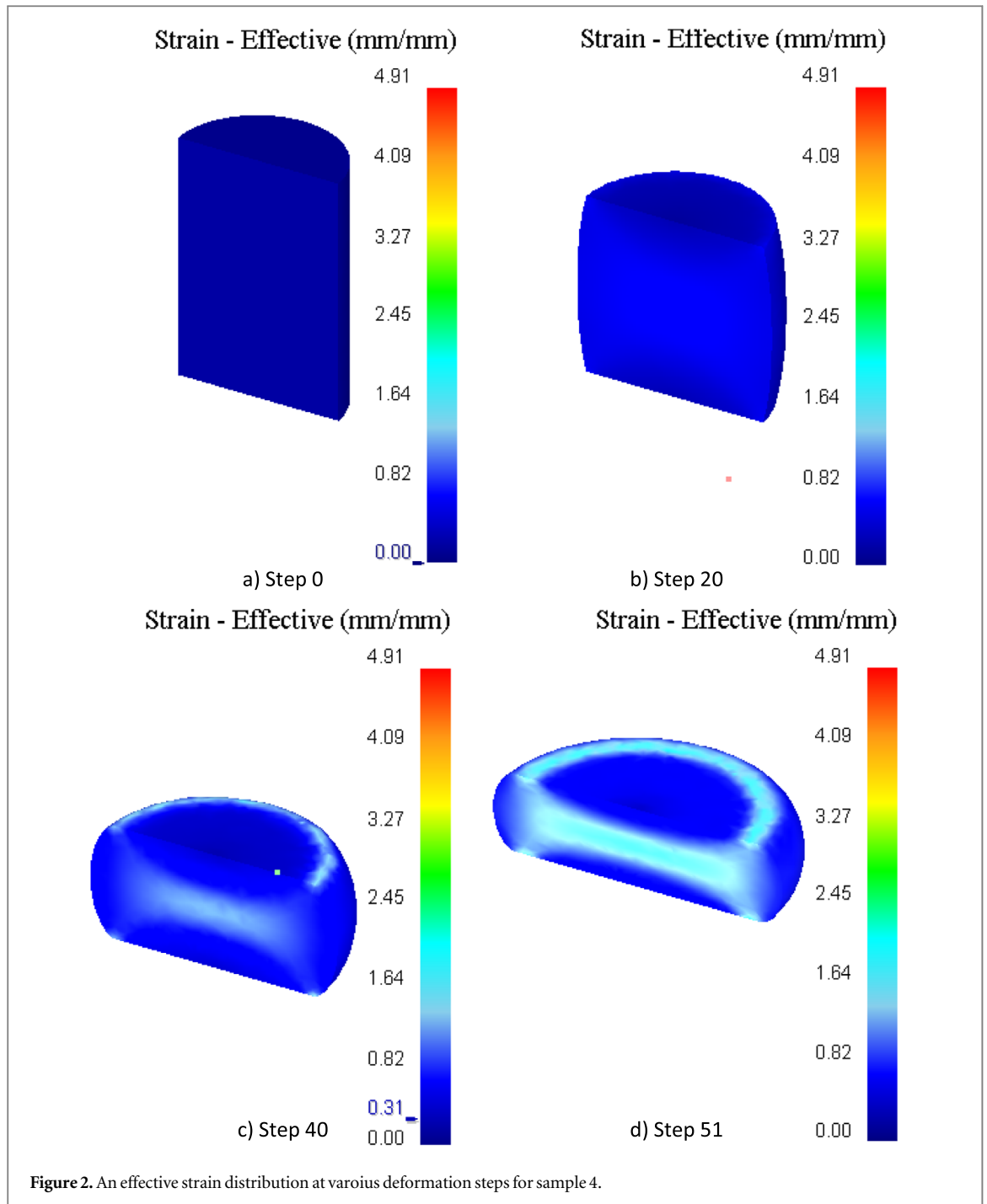
3.2. Flow stress-strain curves

The effective stress-strain curves obtained from point 1, 2 and 3 in the deformed sample after forging simulation are given in figure 3. The maximum effective stress occurred at point 1 as shown in figure 1(b). It was observed that the effective stress increased continuously with an increase in the strain as shown in figure 3(a)). The increase in effective stress can be attributed to the higher amount of dislocation density generated during forging. Hence, work hardening was the dominant deformation mechanism. The maximum effective stress values obtained for the four samples tested were: 241 MPa (sample 1), 242 MPa (sample 2), 232 MPa (sample 3) and 230 MPa (sample 4). The result showed that the maximum effective stress decreased with a decrease in the sample geometry size. At Point 2 and 3, the maximum effective stress increased with a decrease in the sample geometry size. The maximum effective stress values at point 2 were: 150 MPa (sample 1), 156 MPa (sample 2), 163 MPa (sample 3) and 172 MPa (sample 4) as shown in figure 3(b). In the initial stage of forging, the effective stress increased rapidly up to 0.4 strain. This was attributed to high dislocation density, thus increasing resistance to metal flow [19]. At higher strain (>0.4), the flow stress-strain curve attained a steady-state condition. This condition is reached when a balance between work hardening and dynamic softening was attained, leading to

Figure 3. Comparison of effective stress-strain distribution.
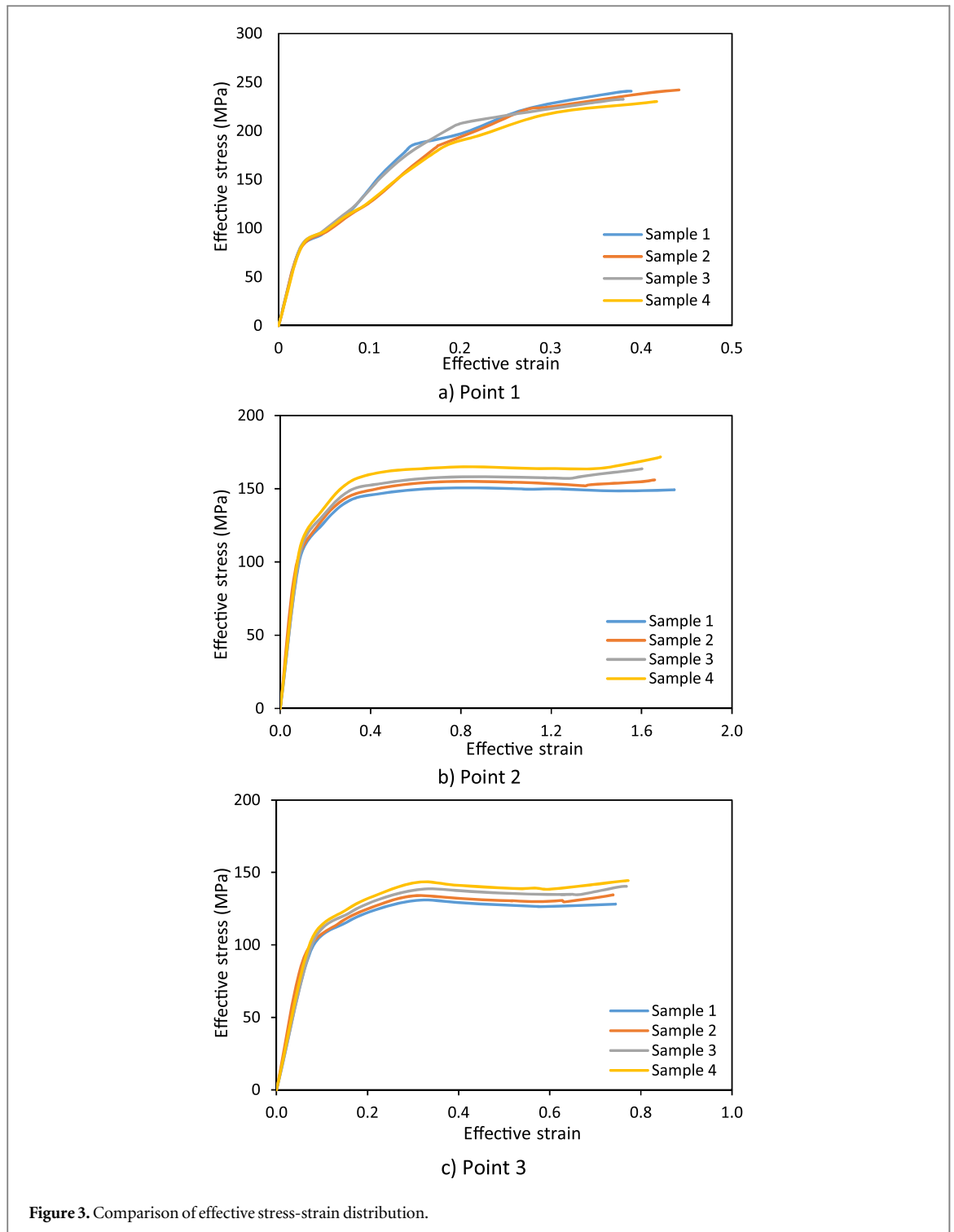
reduced flow stress [20, 21]. The flow stress-strain curves obtained by FEM simulation exhibited similar characteristic behaviour to those obtained from experimental data [22]. The simulation results obtained showed a similar trend to experimental data, hence finite element methods can be used to study metal flow behaviour. At higher strain ($>$1.4), the effective stress increased slightly with an increase in the strain as shown in figure 3(b). This was due to an increase in the friction coefficient at the die-sample contact surface [15]. The maximum effective stress at point 3 showed a similar trend as those obtained at point 2, as shown in figure 3(c). The obtained values were: 130 MPa (sample 1), 134 MPa (sample 2), 140 MPa (sample 3) and 144 MPa (sample 4). The effective stress values of the four samples tested are summarised in table 1. The standard deviation values (table 1) further confirm the variation in effective stress distribution in the samples tested.

In conclusion, the maximum effective stress occurred at point 1 for all tested samples. This point (point 1) had the lowest effective strain in all cases tested. A similar observation of the effective stress and strain

Table 1. Effective stress obtained at three points in the deformed sample.

Point	Effective stress in MPa for each sample				Std. dev
	Sample 1	Sample 2	Sample3	Sample4	
Point 1	241	242	232	230	6.130525
Point 2	150	156	163	172	9.464847
Point 3	130	134	140	144	6.218253

distribution in the deformed sample have been reported in the literature [23]. To this end, it should be pointed out that the sample geometry size affects metal flow behaviour. Therefore, the effective stress obtained is an approximate value. The sample geometry correction factor should be used to correct the stress data values.

4. Conclusion

From the forging simulation, the following conclusions were observed:

1. The maximum effective strain occurred at the centre of the deformed sample for all sample geometry sizes tested. The sample geometry size did not affect the location of the maximum effective strain.

2. The effective stress and strain distribution in the deformed sample were inhomogeneous. The maximum effective stress occurred at the die-sample contact surface. At the contact surfaces, the effective stress decreased with a decrease in the sample geometry size. The effective stress at the centre of the deformed sample increased with a decrease in the sample geometry size.

Data availability statement

Any data that support the findings of this study are included within the article.

ORCID iDs

J Obiko ⓘ https://orcid.org/0000-0002-3069-1581

References

[1] Samantaray D, Mandal S and Bhaduri A 2011 Optimization of hot working parameters for thermo-mechanical processing of modified 9Cr-1Mo (P91) steel employing dynamic materials model *Mater. Sci. Eng.* A **528** 5204–11
[2] George D 1988 *Mechanical Metallurgy* (New York: Mcgraw-Hill Book Company)
[3] Jabbari Taleghani M, Ruiz Navas E, Salehi M and Torralba J 2012 Hot deformation behaviour and flow stress prediction of 7075 aluminium alloy powder compacts during compression at elevated temperatures *Mater. Sci. Eng.* A **534** 624–31
[4] Kishor B, Chaudhari G and Nath S 2016 Hot deformation characteristics of 13Cr-4Ni stainless steel using constitutive equation and processing map *J. Mater. Eng. Perform.* **25** 2651–60
[5] Yang Z, Li Y, Zhang F and Zhang M 2016 Constitutive modeling for flow behavior of medium-carbon bainitic steel and its processing maps *J. Mater. Eng. Perform.* **25** 5030–9
[6] Shokry A, Gowid S and Kharmanda G 2019 Constitutive models for the prediction of the hot deformation behavior of the 10%Cr steel alloy *Materials (Basel)* **12** 1–18
[7] Zhang W, Sha W, Yan W, Wang W, Shan Y and Yang K 2014 Constitutive modeling, microstructure evolution, and processing map for a nitride-strengthened heat-resistant steel *J. Mater. Eng. Perform.* **23** 3042–50
[8] Luan J, Sun C, Li X and Zhang Q 2014 Constitutive model for AZ31 magnesium alloy based on isothermal compression test *Mater. Sci. Technol.* **30** 211–9
[9] Liu C, Zhang R and Yan Y 2011 Hot deformation behaviour and constitutive modelling of P92 heat resistant steel *Mater. Sci. Technol.* **27** 1281–6
[10] Vo P, Jahazi M, Yue S and Bocher P 2007 Flow stress prediction during hot working of near-α titanium alloys *Materials Science and Engineering* A **447** 99–110
[11] Lv C, Zhang L, Mu Z, Tai Q and Zheng Q 2008 3D FEM simulation of the multi-stage forging process of a gas turbine compressor blade *J. Mater. Process. Technol.* **198** 463–70
[12] Obiko J, Mwema F and Bodunrin M 2019 Finite element simulation of X20CrMoV121 steel billet forging process using the Deform 3D software *SN Appl. Sci.* **1** 1–10
[13] Mwema F 2019 Effect of punch force on the upsetting deformation process using three-dimensional finite element analysis *J. Phys. Conf. Ser.* **1378** 032094
[14] Kukuryk M 2018 Numerical analysis of strains and stresses in the hot cogging process *J. Appl. Math. Comput. Mech.* **17** 45–52
[15] Li Y, Onodera E, Matsumoto H and Chiba A 2009 Correcting the stress-strain curve in hot compression process to high strain level *Metall. Mater. Trans. A Phys. Metall. Mater. Sci.* **40** 982–90

[16] Rasti J, Najafizadeh A and Meratian M 2011 Correcting the stress-strain curve in hot compression test using finite element analysis and Taguchi method *Int. J. ISSI* **8** 26–33 (http://journal.issiran.com/article_6374_44b99e06e066fa7ee24705f05935b39d.pdf)

[17] Li X, Wu X, Zhang X and Li M 2013 Dynamic recrystallization of hot deformed 3Cr2NiMnMo steel: modeling and numerical simulation *J. Iron. Steel Res. Int.* **20** 98–104

[18] Antoshchenkov Y and Taupek I 2015 Computer simulation of axisymmetric upsetting *Steel Transl.* **45** 38–41

[19] Zhu L 2018 A two-stage constitutive model of X12CrMoWVNbN10-1-1 steel during elevated temperature *Mater. Res. Express* **5** 1–11

[20] Laasraoui A and Jonas J 1991 Prediction of steel flow stresses at high temperatures and strain rates *Metall. Trans.* A **22** 1545–58

[21] Davenport S, Silk N, Sparks C and Sellars C 2000 Development of constitutive equations for modelling of hot rolling *Mater. Sci. Technol.* **16** 539–46

[22] Qian L, Fang G, Zeng P and Wang L 2015 Correction of flow stress and determination of constitutive constants for hot working of API X100 pipeline steel *Int. J. Press. Vessel. Pip.* **132–133** 43–51

[23] Equbal M, Talukdar P, Kumar V and Ohdar R 2014 Deformation behavior of micro-alloyed steel by using thermo mechanical simulator and finite element method *Procedia Mater. Sci.* **6** no. Icmpc 674–81